2021 IEEE International Conference on Electronics, Computing and Communication Technologies (CONECCT) | 978-1-6654-2849-1/21/$31.00 ©2021 IEEE | DOI: 10.1109/CONECCT52877.2021.9622677

Coarsely Discretized Huygens' Metasurface: Manipulating EM Waves with Simplicity

Abhishek Sharma, *Member, IEEE,* Chu Qi, Kayode A. Oyesina, and Alex M. H. Wong, *Senior Member, IEEE*
State Key Laboratory of Terahertz and Millimeter Waves
Department of Electrical Engineering, City University of Hong Kong, Hong Kong SAR, China
asharma@cityu.edu.hk, (chuqi2-c, kaoyesina2-c)@my.cityu.edu.hk, alex.mh.wong@cityu.edu.hk

***Abstract*—With the genesis of *metamaterials* and its 2D counterpart — *metasurfaces*, there is a paradigm shift in controlling electromagnetic (EM) waves. A special category of metasurfaces known as *Huygens' metasurface* — fundamentally based on equivalence principle, have demonstrated unprecedented capabilities for advanced wavefront engineering. In this paper, we provide current trends and progress in the area of Huygens' metasurfaces, particularly the *coarsely discretized Huygens' metasurfaces*, consisting of two to three meta-atoms per metasurface period. The basic design principle of coarsely discretized metasurface relies on the classical grating theory, where the undesired *Floquet-Bloch* (FB) modes are suppressed by engineering the individual meta-atom, and the desired ones are allowed to radiate in the far-field. Moreover, we briefly summarize the recent development in Huygens' box — a region of space surrounded by an active Huygens' metasurface, and its applications in antenna beam steering. Lastly, we provide a summary and brief outlook on the possible future research directions.**

I. Introduction

Research on artificial materials can be traced back to the late 19^{th} century when Sir J. C. Bose conducted the first experiment in the microwave regime on twisted structures, which are now referred to as the *artificial chiral* elements [1]. In 1948, W. E. Kock has suggested microwave lenses designed by embedding conductive disks, strips, and spheres periodically, resulting in tailored refractive index of the host dielectric medium [2]. He coined the term *artificial dielectrics* for the first time and since then, artificial dielectrics have been the subject of intense research. A comprehensive treatment related to the work on artificial dielectrics' can be found in the classic textbook by R E. Collin [3]. Victor Veselago, in his seminal paper of 1968, has theoretically investigated the wave propagation in the media characterized by a simultaneous negative permittivity and permeability [4]. Over 30 years later, the striking proposal of the perfect lens [5] by Sir John Pendry and the first experimental realization of negative index media at microwave frequencies [6], [7] have given an enormous spark in the field of artificial media, now popularly known as *metamaterials — materials beyond those occurring naturally*.

Metamaterials (MTMs) are 3D structures composed of subwavelength-sized elements (meta-atoms) with engineered EM responses designed to achieve unusual electromagnetic properties. MTMs bring out a new perspective in controlling EM waves, leading to fascinating new physics and exotic phenomena, including negative refraction, invisibility cloaking, optical magnetism, and inverse Doppler effect, among many others [8], [9]. However, despite great success, the challenges in the fabrication of 3D micro-and nano-structures with complex geometries have hindered its utilization in practical applications.

Metasurfaces — 2D counterparts of metamaterials have received enormous attention in the last decade, offering a much better platform to overcome the limitations by bulk metamaterials. Electromagnetic metasurfaces are the planar structures consisting two-dimensional array of meta-atoms or polarizable particles arranged in a periodic or quasi-periodic manner, representing a powerful and versatile tool for controlling EM waves at will [10]–[14]. They have already led to many applications, including anomalous refraction/reflection, flat lenses, polarization control, to name a few. The majority of the metasurfaces design focus on manipulating electric currents only, which gives rise to low transparency and lesser phase coverage for the transmitted waves, greatly limiting the wavefront manipulation capabilities. This led to the establishment of *Huygens' metasurface* (HMS) [15], [16], which is fundamentally based on the classical Schelkunoff's equivalence principle – a generalization of the Huygens' principle dating back to the late 17^{th} century [17]. HMS has seen unprecedented growth over the past lustrum due to its exceptional capabilities to transform EM waves in a reflectionless manner [18]–[24].

One of the standard metasurface design schemes follows the surface impedance-admittance approach that conforms to the generalized sheet transition condition between an incident and the desired electromagnetic fields [24]. The continuous impedance-admittance surface is then finely discretized and realized using the metallic or dielectric meta-atoms with predefined EM response. A typical discretization of the metasurface accommodates 8 to 15 meta-atoms per period or, in some cases, per wavelength [20], [25]. The metasurface comprising densely packed deeply subwavelength-sized meta-atoms is subject to implementation difficulties, especially for the millimeter-wave (mm-wave) frequencies and beyond.

Recently, the idea of *coarse discretization* has been conceived to design uncomplicated, cost-effective, robust yet efficient metasurface without the need for deeply subwavelength-sized meta-atoms. The *coarsely discretized metasurface* (CDMS) consists of one [26]–[28] or a few elements [29]–

[34] per period to effectively tailor the impinging wavefront. The design of CDMS exploits the diffraction grating physics, and when illuminated by an incident wave, discrete sets of propagating and evanescent *Floquet-Bloch* (FB) modes are excited following the periodicity of the structure. The meta-atoms are engineered to suppress the undesired propagating modes and allowing the desired ones to radiate in the far-field. In addition, the sparsely discretized metasurface subdue the fabrication difficulties even at the millimeter wave frequencies and beyond.

This paper describes recent advances in the coarsely discretized Huygens' metasurface, which features two to three elements per metasurface period. Moreover, we summarize recent progress in the area of Huygens' box with its application in antenna beam steering. This review paper by no means is exhaustive, and the following sections describe the work carried out in the author's research group.

II. Metasurface Discretization

A periodic metasurface with period Λ_g and spatial frequency $k_g = \frac{2\pi}{\Lambda_g}$ is considered in free-space, which scatters an incoming plane wave into a discrete set of FB modes. The transverse spatial frequencies of these FB modes are expressed as

$$k_{yn} = k_{yi} + nk_g = k_{yi} + n\frac{2\pi}{\Lambda_g}, \tag{1}$$

where k_{yi} is the y-directed spatial frequency of the incident wave, n $(= 0, \pm1, \pm2, \cdots)$ represents the FB mode number. Fig. 1 shows the operation of a periodic metasurface in the k-space domain, which can be enunciated mathematically as

$$\Pi_o(k_y) = \sum_n a_n \delta(k_y - k_{yn}) \tag{2}$$

where, $\Pi_o(k_y)$ represents the output k-space spectrum, a_n represents the amplitude, and k_{yn} is the transverse spatial frequency of the n^{th} FB mode given by (1). It is to be noted that the arrows in Fig. 1 indicate the presence of spectral components but do not provide any phase and amplitude information of these spectral components. In the k-space domain, there exist an infinite number of FB modes; however, only a finite number of these modes which falls in the range of $k_y \in [-k_0, k_0]$ (represented by a purple box in Fig. 1) can diffract into the far-field. The range of k_y as mentioned before is known as *propagation range*, and the modes that lie outside this range will become evanescent. Wong and Eleftheriades in [29] have described that *N*-fold discretization

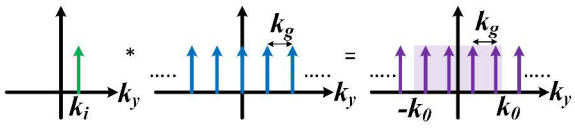

Fig. 1. k-space operation of a periodic metasurface. Arrows denote possible spectral components' spatial frequencies but do not provide information about the amplitude and phase. The violet box indicates the propagation regime.

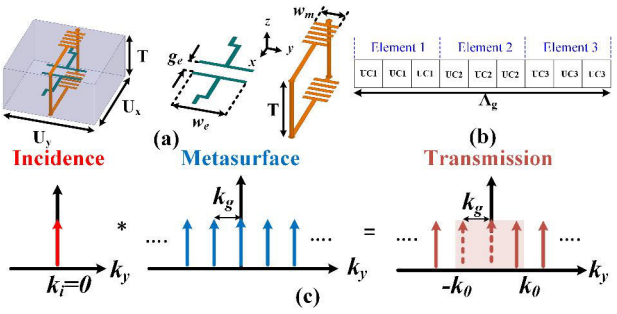

Fig. 2. (a) Geometry of the Huygens' meta-atom, comprising three stacked layer with metallic inclusion. (b) A diagram depicting one period (Λ_g) of the metasurface. (c) k-space operation of refracting metasurface. Reproduced figure from [31].

within the metasurface period is adequate to determine *N* FB modes that radiate into the far-field. Underlying this concept, a perfect anomalous reflector [29] and retroreflector [30] has been designed.

III. Coarsely Discretized Huygens' Metasurface

Huygens' metasurface consist of co-located orthogonal electric and magnetic polarizable particles, which form the 2D array of Huygens' sources, resulting in unidirectional scattering and full 2π phase control. Next, we provide three examples of Huygens' metasurface for anomalous transmission, consisting of metallic and dielectric particles.

A. Huygens' Metasurface with Metallic Inclusion: Stacked-Layer Topology

Stacked-layer meta-atom, constructed by stacking multiple dielectric layers together with metallic inclusion, is the most celebrated and utilized unit-cell topology [20], [21]. In [31], a coarsely discretized metasurface is realized using aforementioned topology, where different metallic strips are printed on multiple substrate layers having same relative permittivity, as shown in Fig. 2(a). The loaded-dipole on the middle layer acts as an electric dipole, whereas the loop for realizing the magnetic dipole is formed by connecting the metallic strip located on the top and bottom layer through vias. In this way, a Huygens' meta-atom is approximated by orthogonal co-located electric dipole (loaded-dipole) and magnetic dipole (loop). The metasurface is designed to operate for normal incidence, considering the manipulation of first three FB modes *i.e.* $n = 0$ and $n = \pm1$, where these modes are excited in both reflection and transmitted regimes. The nature of the Huygens' metasurface is such that it should ideally suppress the reflection modes; however, these modes are excited weakly. By properly engineering the meta-atom all the undesired FB modes (T_{-1}, T_0 R_0, and $R_{\pm1}$ are suppressed and the power is maximized into the desired mode *i.e.* T_1, where T stands for transmission and R denotes reflection.

In this case, a coarse discretization level of three elements per metasurface period is ample for the mode manipulation. It is to be noted that each of the three elements composed of three identical unit-cells, as shown in Fig. 2(b). Fig. 2(c) shows

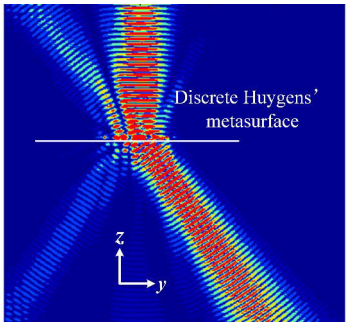

Fig. 3. Electric field distribution at 10 GHz, showing anomalous refraction for normal incidence Gaussian beam. Reproduced figure from [31].

the *k*-space operation of the refracting metasurface. The period of metasurface is set as $\lambda_0 < \Lambda_g < 2\lambda_0$ (in the present case $\Lambda_g = 1.8\lambda_0$, where λ_0 is calculated at 10 GHz) to eliminate the higher order ($n \geq 2$) FB modes. Fig. 3 shows the electric field distribution at 10 GHz along the yz-plane. Examining the plot, it is clear that the normal incident Gaussian beam is anomalously refracted. Simulation results shows that more than 70% of the incident power is re-routed to the desired direction. The refracted angle (θ_r) can be calculated using the following equation,

$$\sin\theta_r = \sin\theta_i + \frac{n\lambda_0}{\Lambda_g} \tag{3}$$

where n is the mode number, θ_i is the incident angle and Λ_g is the metasurface period. Taking $\Lambda_g = 1.8\lambda_0$, $n = 1$, and $\theta_i = 0°$, the refracted angle calculated using (3) is $33.7°$.

B. Dielectric Huygens' Metasurface

In general, the realization of HMS comprising metallic particles either require stacked topology [20], [21] or wire-loop configuration [22]. Such requirements lead to fabrication difficulties, particularly for the high-frequency spectrum. Moreover, the unavoidable ohmic losses at high frequencies such as mm-wave, degrade the efficiency of the meta-devices. On the contrary, dielectric Huygens' metasurface (DHMS), comprising high index and low-loss dielectric particles, has been suggested as an alternative path for wavefront manipulation [25], [32]–[36]. The DHMS is characterized by the spectral overlapping of electric and magnetic dipoles or quadrupoles in a single dielectric particle, providing unidirectional scattering and 2π phase coverage. Next, we show two examples of coarsely discretized DHMSs for anomalous refraction under normal and oblique angle of incidence.

1) Normal Incidence: The dielectric meta-atom placed in xy-plane (refer inset of Fig.4(a)) is simulated using the periodic boundary conditions and Floquet ports. The relative permittivity of the DR is 12 and the dielectric losses are not included in the simulations. The structure is illuminated by a TE-polarized (electric field is along x-direction) plane wave propagating along negative z-direction. Upon normal incidence, two transmission minimas are observed at 56.2 GHz and 64.4 GHz (refer Fig. 4(a)). Observing the electric field distribution at the frequencies mentioned above, it is clear that at 56.2 GHz, a y-directed magnetic dipole is excited (refer Fig. 4(c)), whereas, at 64.4 GHz, an electric dipole is excited oriented along x-direction (refer Fog. 4(d)). Next, we optimize the geometrical parameters (L_x, L_y, and H) of the dielectric block so that both the dipolar modes get overlapped to form a Huygens' source. This resulted in enhanced transmission and $360°$ phase coverage, as shown in Fig. 4(e) [33]. The optimized dimensions are: $L_x = 2.70$, $L_y = 1.70$, and $H = 0.80$ (all dimensions are in millimeters).

As described previously, only three elements are sufficient in order to manipulate the first three FB modes *viz.* $n = 0$, and $n = \pm 1$, and thus, a transmissive metasurface at 60GHz is designed utilizing three spatially varying dielectric Huygens' meta-atom per metasurface period (refer Fig. 5(a)) [33]. The period of the metasurface, in this case, is $\Lambda_g = 1.74\lambda_0$. Fig. 5(b) illustrates the transformation of y-directed spatial frequency of the plane wave as it refracts from a refracting metasurface. Figs. 5(c) and 5(d) depicts the transmission and reflection magnitude plots for the three-element DHMS. Examining the transmitted and reflected modes, it is clear that the transmission is maximized to the desired T_{-1} mode at 60 GHz, whereas the undesired modes both in reflection (R_0, R_{+1}, R_{-1}) and transmission regime (T_0, T_{+1}) are suppressed. In this case, $> 80\%$ of the total transmitted power is contained in the desired FB mode. Fig. 5(e) shows the electric field distribution illustrating the anomalous refraction at 60GHz. The refracted angle (θ_r) calculated using (3) under normal incidence for $n = -1$ and $\Lambda_g = 1.74\lambda_0$ is $-35°$.

2) Oblique Incidence: We seek to design a transmissive metasurface operating under oblique incidence, considering the manipulation of only two FB modes *i.e.* the specular mode ($n = 0$) and the first higher-order mode ($n = -1$). Therefore, in this case, a binary discretization will suffice for controlling the FB modes mentioned above. We termed the resultant metasurface as *binary dielectric Huygens' metasurface* (B-DHMS) [34]. The metasurface period is chosen so that only the fundamental ($n = 0$) and first higher-order ($n = -1$) modes are propagating. The *k*-space operation of B-DHMS is illustrated in Fig. 6(a).

In this section, we provide a design of refracting metasurface at 60 GHz based on the procedure outlined in [34]; but using a different unit-cell geometry. Firstly, we characterize the meta-atom (refer inset of Fig. 6(b)) arranged in an infinite periodic array for the normal incident angle. The full-wave simulation shows that the dielectric block under consideration produces electric and magnetic dipole resonance at 56.1 GHz and 58.8 GHz, respectively (figures omitted for brevity). The geometrical parameters of the rectangular dielectric are then optimized to achieve the spectral overlapping of two dipolar modes, which results in unidirectional scattering and full 2π phase coverage. It is worth mentioning here that the unit-cell designed for normal incidence is not directly applicable for oblique incident angle. When the incident angle deviates from normal, the transmission magnitude starts decreasing, and thus, a slight dimensional modification is required to regain

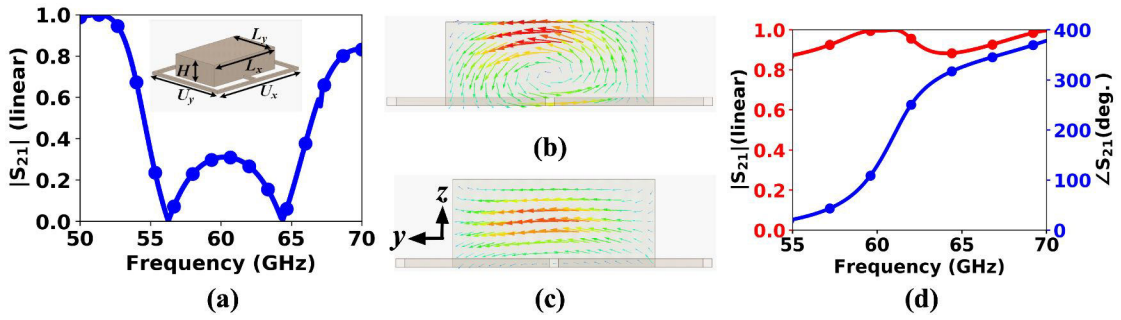

Fig. 4. (a) Transmission response of the dielectric meta-atom. Inset shows the schematic of dielectric meta-atom (b) Electric field distribution at 56.2 GHz, representing magnetic dipole oriented along y-direction. (c) Electric field distribution at 64.4 GHz, showing x-directed electric dipole. (d) Transmission spectra of dielectric Huygens' meta-atom.

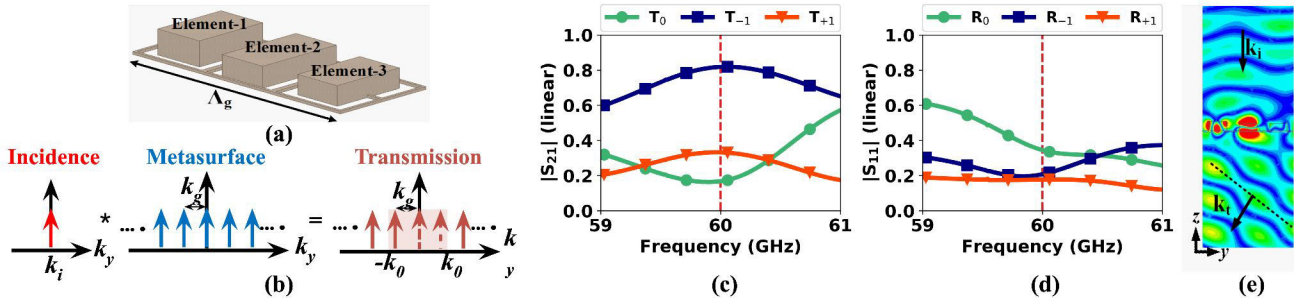

Fig. 5. (a) Isometric view of three-element refracting metasurface ($\Lambda_g = 1.74\lambda_0$). (b) k-space operation of the metasurface. (c) Transmission magnitude. (d) Reflection magnitude. (e) E-field distribution at 60 GHz, illustrating anomalous transmission. Sub-figures (a, b, and e) reproduced from [33].

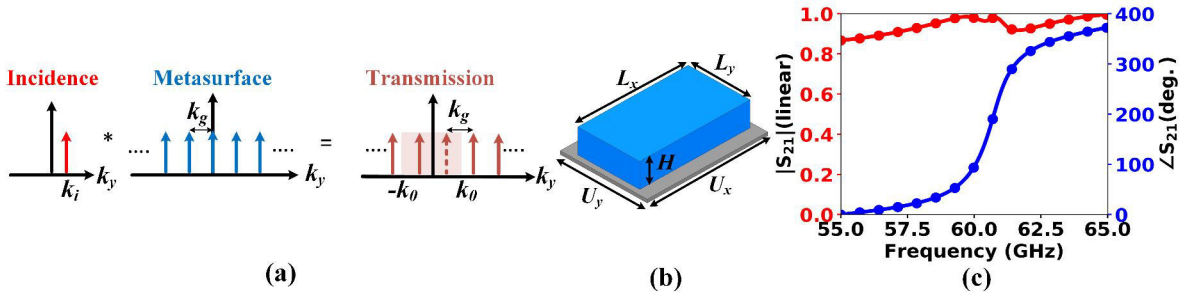

Fig. 6. (a) k-space operation of B-DHMS. (b) Geometry of the rectangular dielectric meta-atom ($U_x = 0.72\lambda_0$ and $U_y = 0.52\lambda_0$, where λ_0 is calculated at 60 GHz). (c) Transmission spectra of dielectric Huygens' meta-atom under oblique incidence of 15°.

the spectral overlapping for oblique incidence. In this case, we consider the incident plane wave to be TE-polarized (x-directed electric field) and propagating along the yz-plane. Fig. 6(c) shows the transmission spectrum for oblique incidence of 15°, showing transmission > 0.9 (linear scale) and phase coverage of 2π. B-DHMS is then realized by placing two meta-atoms having a phase difference of 180° adjacent to each other, as depicted in Fig. 7(a). Fig. 7(b) shows the transmission and reflection magnitude plots for B-DHMS. Examining the transmitted modes, it is clear that the transmission to the desired T_{-1} mode is maximized, whereas the specular mode (T_0) is suppressed along with the reflection modes (R_0, R_{-1}). The electric field distribution shown in Fig. 7(c) depicts the anomalous refraction phenomenon under oblique incidence. The refracted angle θ_r calculated using (3), for $n = -1$ and $\Lambda_g = 1.04\lambda_0$ is $-44.5°$. Further, the refracted efficiency — defined as the ratio of the scattered power in the desired mode to the total scattered power, of B-DHMS is 87% at 60 GHz.

IV. Huygens' Box Antenna

Recently, the concept of Huygens' Box–a rectangular metallic cavity lined by a simple active Huygens' metasurface, has been proposed for arbitrary EM waveform generations inside the enclosed area [37]. Traveling waves and Bessel waves has been generated inside a metallic cavity utilizing the same metasurface by aptly controlling the source excitations [37]–[41]. Next, we briefly describe one of the promising applications of Huygens' box *i.e.* antenna beam steering.

Fig. 8(a) shows the schematic of the TM1 Huygens' box antenna [42], consisting of two-layers of Huygens' metasurface elements wrapped around a region of interest and directed along z-axis. This arrangement can be used to generate TM1

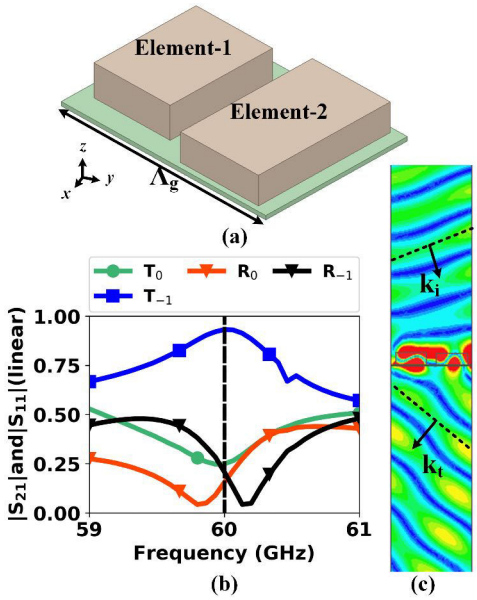

Fig. 7. (a) Isometric view of two-element refracting metasurface ($\Lambda_g = 1.04\lambda_0$) (b) Transmission and reflection coefficients. (c) E-field distribution in yz-plane at 60 GHz, illustrating anomalous refraction.

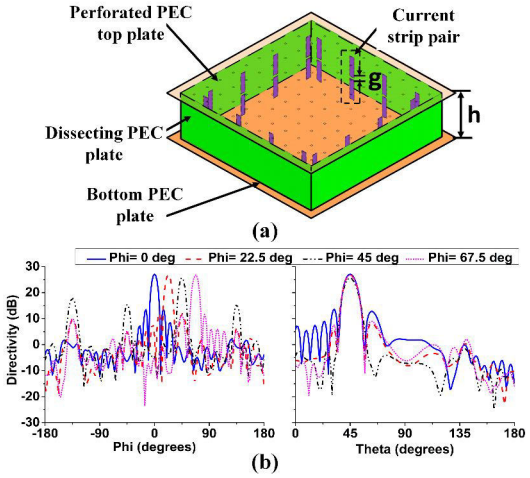

Fig. 8. (a) Geometry of the TM1 Huygens' box antenna. (b) Radiation pattern showing the azimuth beam steering at 60 GHz for TM1 Huygens' box antenna. The patterns are depicted for four wave propagation direction *i.e.* $\phi = 0^\circ,\ 22.5^\circ,\ 45^\circ,\ 67.5^\circ$. The left panel shows the pattern at $\theta = 45^\circ$ plane and the right panel depicts pattern in $\phi = 0^\circ,\ 22.5^\circ,\ 45^\circ,\ 67.5^\circ$ planes. Reproduced figure from [42].

traveling waves, and the desired radiation is formed by allowing the leakage of generated cavity waves through perforations created on the top plate of the cavity. It is worth mentioning here that these perforations do not affect the radiation pattern as far as these are deeply subwavelength ($0.025\lambda_0 \times 0.025\lambda_0$) and evenly spaced ($0.125\lambda_0$) [42]. The HBA dramatically reduces the number of elements as compared to the traditional patch antenna array of equivalent aperture size, without much compromising the directivity and sidelobe levels. Fig. 8(b) depicts azimuth beam steering for $0^\circ \leq \phi < 90^\circ$. The slightly stronger sidelobe levels observed when ϕ approaches 45° is a consequence of the imperfect plane wave generation in Huygens' box. A further reduction on the number of sources is possible using TEM mode of operation with a low refractive index MTM [42], [43].

V. Conclusion and Outlook

Huygens' metasurfaces (HMSs) are emanating as an extraordinary platform for extreme EM wave manipulation. These engineered surfaces are based on the classical equivalence principle and consist of metallic or dielectric Huygens' scatterers – encompassed by the orthogonal co-located electric and magnetic dipoles. The versatile nature of HMSs can be employed to control the phase, amplitude, and polarization of an incoming EM wave. Combining the concept of coarse discretization with HMSs, provides new opportunities for controlling EM waves with simplicity and high efficiency. The coarsely discretized metasurfaces overcome the fabrication difficulties at high frequencies such as mm-wave and terahertz, where it is highly non-trivial to fabricate the meta-devices due to their smaller feature sizes.

This review provided a few demonstrations of coarsely discretized metallic and dielectric Huygens' metasurfaces for anomalous refraction under normal and oblique incidence. Another example includes the arbitrary EM wave generation inside a cavity surrounded by active HMS–the Huygens' box. We have shown one of the promising 5G application *i.e.* beam steering using Huygens' box antenna, which dramatically reduces the number of elements as compared to the traditional microstrip patch antenna array of similar aperture size.

Lastly, we would like to mention some promising future research directions based on our perspectives. While a good efficiency has been achieved for anomalous refraction, exciting opportunities still exist for future studies. For instance, the metasurface bandwidth is $\approx 5-10\%$, which significantly restricts its functionality for broadband applications. This opens up a new avenue to design metasurfaces that will provide broadband operation with high efficiency. Another emerging area is that of broadband achromatic metalenses with good efficiency. More exciting opportunities exist for active/re-configurable Huygens' metasurface. For example, the area of superoscillations is beneficial for super-resolution electromagnetic focusing and imaging. The Huygens' box's exceptional capabilities show the potential for realizing a superoscillatory focal spot (beating the diffraction limit) without using evanescent waves. As the Huygens' box enables one to synthesize and control an arbitrary EM wave inside an enclosed area, it may find potential applications in the medical sector such as magnetic resonance imaging [44]. With far-reaching implications of coarsely discretized metasurfaces, we envisage its impactful application in the area of acoustic metasurfaces to manipulate the sound waves with simplicity. Furthermore, this concept can be extended to realize simple and robust dual-physics meta-devices that can simultaneously control electromagnetic and acoustic waves. The incessant evolution of fundamental concepts and potential applications

makes this field a rapidly expanding frontiers of *surface electromagnetics*, and still there are lot many things to be discovered.

VI. Acknowledgement

This work is supported by an Early Career Scheme from the Research Grants Council of the Hong Kong under Grant 21211619.

References

[1] J. C. Bose, "On the rotation of plane of polarisation of electric wave by a twisted structure," *Proc. R. Soc. Lond.*, vol. 63, pp. 146–152, 1898.

[2] W. E. Kock, "Metallic delay lenses," *The Bell System Technical Journal*, vol. 27, no. 1, pp. 58–82, 1948.

[3] R. E. Collin, *Field Theory of Guided Waves*, 2nd ed. Wiley-IEEE Press, 1990, ch. 12.

[4] V. G. Veselago, "The electrodynamics of substances with simultaneous negative values of ϵ and μ," *Soviet Physics Uspekhi*, vol. 10, no. 4, pp. 509–514, 1968.

[5] J. B. Pendry, "Negative refraction makes a perfect lens," *Phys. Rev. Lett.*, vol. 85, pp. 3966–3969, 2000.

[6] D. R. Smith, W. J. Padilla, D. C. Vier *et al.*, "Composite medium with simultaneously negative permeability and permittivity," *Phys. Rev. Lett.*, vol. 84, pp. 4184–4187, 2000.

[7] R. A. Shelby, D. R. Smith, and S. Schultz, "Experimental verification of a negative index of refraction," *Science*, vol. 292, no. 5514, pp. 77–79, 2001.

[8] G. V. Eleftheriades and K. G. Balmain, *Negative-Refraction Metamaterials: Fundamental Principles and Applications*. Wiley-IEEE Press, 2005.

[9] N. Engheta and R. W. Ziolkowski, Eds., *Metamaterials: Physics and Engineering Explorations*. Wiley-IEEE Press, 2006.

[10] F. Yang and Y. Rahmat-Samii, Eds., *Surface Electromagnetics: With Applications in Antenna, Microwave, and Optical Engineering*. Cambridge University Press, 2019.

[11] N. Yu, P. Genevet, M. A. Kats *et al.*, "Light propagation with phase discontinuities: Generalized laws of reflection and refraction," *Science*, vol. 334, no. 6054, pp. 333–337, 2011.

[12] O. Quevedo-Teruel, H. Chen, A. Díaz-Rubio *et al.*, "Roadmap on metasurfaces," *J. Opt.*, vol. 21, no. 7, p. 073002, 2019.

[13] N. Mohammadi Estakhri and A. Alù, "Wave-front transformation with gradient metasurfaces," *Phys. Rev. X*, vol. 6, p. 041008, Oct 2016.

[14] W. T. Chen, A. Y. Zhu, and F. Capasso, "Flat optics with dispersion-engineered metasurfaces," *Nat. Rev. Mater.*, vol. 5, pp. 604–620, 2020.

[15] C. Pfeiffer and A. Grbic, "Metamaterial Huygens' surfaces: Tailoring wave fronts with reflectionless sheets," *Phys. Rev. Lett.*, vol. 110, p. 197401, 2013.

[16] M. Selvanayagam and G. V. Eleftheriades, "Discontinuous electromagnetic fields using orthogonal electric and magnetic currents for wavefront manipulation," *Opt. Express*, vol. 21, no. 12, pp. 14 409–14 429, 2013.

[17] C. Huygens, *Traitè de la lumiere*. Leiden: Pieter van der Aa, 1690, translated by Silvanus P. Thompson as Treatise on Light (London: Macmillan, 1912; Project Gutenberg edition, 2005).

[18] M. Chen, M. Kim, A. M. H. Wong *et al.*, "Huygens' metasurfaces from microwaves to optics: a review," *Nanophotonics*, vol. 7, no. 6, pp. 1207–1231, 2018.

[19] F. S. Cuesta, I. A. Faniayeu, V. S. Asadchy *et al.*, "Planar broadband Huygens' metasurfaces for wave manipulations," *IEEE Trans. Antennas Propag.*, vol. 66, no. 12, pp. 7117–7127, 2018.

[20] M. Chen, E. Abdo-Sánchez, A. Epstein *et al.*, "Theory, design, and experimental verification of a reflectionless bianisotropic Huygens' metasurface for wide-angle refraction," *Phys. Rev. B*, vol. 97, p. 125433, Mar 2018.

[21] J. P. Wong, M. Selvanayagam, and G. V. Eleftheriades, "Design of unit cells and demonstration of methods for synthesizing Huygens' metasurfaces," *Photonics Nanostructures: Fundam. Appl*, vol. 12, no. 4, pp. 360–375, 2014.

[22] M. Chen and G. V. Eleftheriades, "Omega-bianisotropic wire-loop huygens' metasurface for reflectionless wide-angle refraction," *IEEE Trans. Antennas Propag.*, vol. 68, no. 3, pp. 1477–1490, 2020.

[23] A. E. Olk and D. A. Powell, "Huygens metasurface lens for W-band switched beam antenna applications," *IEEE Open Journal of Antennas and Propagation*, vol. 1, pp. 290–299, 2020.

[24] V. G. Ataloglou, M. Chen, M. Kim *et al.*, "Microwave huygens' metasurfaces: Fundamentals and applications," *IEEE Journal of Microwaves*, vol. 1, no. 1, pp. 374–388, 2021.

[25] M. K. Emara, T. Tomura, J. Hirokawa *et al.*, "All-dielectric huygens' metasurface pair for mm-wave circularly-polarized beam-forming," in *2020 14th European Conference on Antennas and Propagation (EuCAP)*, 2020, pp. 1–4.

[26] Y. Ra'di, D. L. Sounas, and A. Alù, "Metagratings: Beyond the limits of graded metasurfaces for wave front control," *Phys. Rev. Lett.*, vol. 119, p. 067404, 2017.

[27] V. Popov, F. Boust, and S. N. Burokur, "Beamforming with metagratings at microwave frequencies: Design procedure and experimental demonstration," *IEEE Trans. Antennas Propag.*, vol. 68, no. 3, pp. 1533–1541, 2020.

[28] O. Rabinovich and A. Epstein, "Arbitrary diffraction engineering with multilayered multielement metagratings," *IEEE Trans. Antennas Propag.*, vol. 68, no. 3, pp. 1553–1568, 2020.

[29] A. M. H. Wong and G. V. Eleftheriades, "Perfect anomalous reflection with a bipartite Huygens' metasurface," *Phys. Rev. X*, vol. 8, p. 011036, 2018.

[30] A. M. H. Wong, P. Christian, and G. V. Eleftheriades, "Binary huygens' metasurfaces: Experimental demonstration of simple and efficient near-grazing retroreflectors for TE and TM polarizations," *IEEE Trans. Antennas Propag.*, vol. 66, no. 6, pp. 2892–2903, 2018.

[31] C. Qi and A. M. H. Wong, "A coarsely discretized Huygens' metasurface for anomalous transmission," in *2019 IEEE Asia-Pacific Microwave Conference (APMC)*, 2019, pp. 935–937.

[32] A. Sharma and A. M. H. Wong, "Towards efficient EM wave manipulation using a discrete dielectric huygens' metasurface," in *2020 14th European Conference on Antennas and Propagation (EuCAP)*, 2020, pp. 1–3.

[33] ——, "Controlling wavefront using a coarsely discretized dielectric Huygens' metasurface," in *2020 IEEE International Symposium on Antennas and Propagation and North American Radio Science Meeting*, 2020, pp. 753–754.

[34] ——, "Sparsely discretized refracting dielectric huygens' metasurface at 28 GHz," in *2020 IEEE Asia-Pacific Microwave Conference (APMC)*, 2020, pp. 1027–1029.

[35] M. Decker, I. Staude, M. Falkner *et al.*, "High-efficiency dielectric Huygens' surfaces," *Adv. Opt. Mater.*, vol. 3, no. 6, pp. 813–820, 2015.

[36] I. Staude, T. Pertsch, and Y. S. Kivshar, "All-dielectric resonant meta-optics lightens up," *ACS Photonics*, vol. 6, no. 4, pp. 802–814, 2019.

[37] A. M. H. Wong and G. V. Eleftheriades, "Active huygens' box: Arbitrary electromagnetic wave generation with an electronically controlled metasurface," *IEEE Trans. Antennas Propag.*, vol. 69, no. 3, pp. 1455–1468, 2021.

[38] ——, "A simple active huygens source for studying waveform synthesis with huygens metasurfaces and antenna arrays," in *2015 IEEE International Symposium on Antennas and Propagation USNC/URSI National Radio Science Meeting*, 2015, pp. 1092–1093.

[39] ——, "Active Huygens' metasurfaces for RF waveform synthesis in a cavity," in *2016 18th Mediterranean Electrotechnical Conference (MELECON)*, 2016, pp. 1–5.

[40] A. M. H. Wong and G. V. Eleftheriades, "Experimental demonstration of the Huygens' box: Arbitrary waveform generation in a metallic cavity," in *2018 IEEE International Symposium on Antennas and Propagation USNC/URSI National Radio Science Meeting*, 2018, pp. 1893–1894.

[41] K. A. Oyesina, O. Z. Aly, G. G. L. Zhou *et al.*, "Active Huygens' box: Arbitrary synthesis of EM waves in metallic cavities," in *2019 International Applied Computational Electromagnetics Society Symposium (ACES)*, 2019, pp. 1–2.

[42] K. A. Oyesina and A. M. H. Wong, "Metasurface-enabled cavity antenna: Beam steering with dramatically reduced fed elements," *IEEE Antennas Wireless Propag. Lett*, vol. 19, no. 4, pp. 616–620, 2020.

[43] ——, "Metamaterial-loaded Huygens' box antenna: Highly-directive beam steering with very few phasing elements," in *2020 IEEE Asia-Pacific Microwave Conference (APMC)*, 2020, pp. 284–286.

[44] C. Xue, G. G. L. Zhou, and A. M. H. Wong, "Improving homogeneity for MRI RF field at 3T using a Huygens' box," in *2020 IEEE International Symposium on Antennas and Propagation and North American Radio Science Meeting*, 2020, pp. 915–916.